Available online at www.sciencedirect.com
SCIENCE DIRECT®
Physics and Chemistry of the Earth 31 (2006) 428–436
PHYSICS and CHEMISTRY of the EARTH
www.elsevier.com/locate/pce

Seismo-electromagnetic phenomenon in terms of 3D vector problem of subionospheric radio wave propagation across the solar terminator

O.V. Soloviev [a,*], M. Hayakawa [b], O.A. Molchanov [c]

[a] Institute of Radio Physics, St. Petersburg State University, Ul'yanovskaya 1/1, Petrodvorets, St. Petersburg 198504, Russia
[b] Department of Electronic Engineering, The University of Electro-Communications, 1-5-1 Chofugaoka, Tokyo 182-8585, Japan
[c] United Institute of Physics of the Earth RAS, Bol. Gruzinskaya 10, Moscow 123810, Russia

Accepted 6 February 2006
Available online 24 May 2006

Abstract

This paper presents a further development of mathematical model, an asymptotic theory and an appropriate numerical algorithm to study the vector VLF point source field propagation problem within the non-uniform Earth–ionosphere waveguide. It is the sequential development of our previous article [Soloviev, O.V., Hayakawa, M., Ivanov, V.I., Molchanov, O.A., 2004. Seismo-electromagnetic phenomenon in the atmosphere in terms of 3D subionospheric radio wave propagation problem. Phys. Chem. Earth 29, 639–647. doi:10.1016/j.pce.2003.10.002]. We have taken into account 3D local anisotropic ionosphere inhomogeneity over the ground of the solar terminator transition. The local ionosphere inhomogeneity, whose centre is situated above the model earthquake, is simulated by a bell-shaped tensor impedance perturbation of the ionospheric waveguide wall. The various propagation paths, which cut across the terminator line at different angles, have been investigated. Numerical results show that the emergence of the local ionosphere inhomogeneity on the radio wave propagation across the solar terminator path deforms the curves of field amplitude and phase diurnal variations in accord with the experimental observational data.

Keywords: 3D radio wave propagation problem; Local ionosphere inhomogeneity; Solar terminator; Seismic event—lower ionosphere interaction

1. Introduction

Investigations of electromagnetic effects of earthquakes are currently being carried out by many diverse groups in many different countries within various sub-disciplines of geophysics and radio physics. Among these researches we would like to particularly mention a group interested in studying the anomalies in electromagnetic fields of VLF radio stations, conterminous on time with earthquakes, whose epicentres are located in the vicinity of radio wave propagation path (so-called VLF remote sensing). Such anomalies in amplitude and phase of radio signals can be explained by change of conditions on the path of radio wave propagation, namely, in the vicinity of an epicentre of earthquake both on the ground and in the lower ionosphere. This radio wave band does not feel any variations in the air environment. In the context of VLF radio wave propagation the most important ionospheric parameters are electron density $N_e(z)$ and effective collision frequency $\nu_e(z)$ altitude profiles. These parameters in regular conditions are determined by solar zenith angle. The spatially localized variations of electron density (due to various causes) are possible in perturbed conditions.

The possibility of existence of ionospheric earthquake precursory anomalies is still widely debated in the science community. There are several reasons for this cautious assessment, among them a lack of understanding of the link between the seismo-mechanical processes in the ground and the atmospheric/ionospheric and electromagnetic events. At the same time various ionospheric plasma phenomena, for example ionospheric turbulence, have been detected by satellites and ground-based facilities over the epicentre of future shocks (Hayakawa and Molchanov,

* Corresponding author. Tel./fax: +7 812 428 7289.
E-mail address: soloviev@os1121.spb.edu (O.V. Soloviev).

1474-7065/$ - see front matter © 2006 Elsevier Ltd. All rights reserved.
doi:10.1016/j.pce.2006.02.038

2002; Hobara et al., 2005). It seems rather perspective for us to consider as a source of ionospheric earthquake precursory anomalies the atmospheric gravity waves generated on the ground (Lizunov and Hayakawa, 2004).

We shall not deal with a problem of occurrence of ionospheric inhomogeneities, but the aim of this paper is the mathematical modelling of the situation recorded during the January 1995 experiment (Hayakawa et al., 1996a,b), assuming that a local inhomogeneity arises in lower ionosphere during the stage prior to an earthquake. In that light, the object of present paper does not differ from our previous paper (Soloviev et al., 2004), however, now it will be the solution of vector radio wave propagation problem on the basis of the new technique developed by Soloviev (2005), unlike the previous in which the scalar radio wave propagation problem statement has been used.

In the following we will simulate the result of experiment. Monitoring of the "OMEGA" signals at the Inubo observatory (35°42′ N; 140°52′ E) from the Tsushima transmitter (34°37′ N; 129°27′ E) at both 10.2 and 11.3 kHz frequencies revealed a time shift of the regular minima in the diurnal variations of phase and amplitude (Hayakawa et al., 1996a; Molchanov and Hayakawa, 1998; Molchanov et al., 1998) on the propagation path 1043 km long, which has passed near epicentre of the great Hyogo-ken Nambu (Kobe) earthquake (January 17, 1995). Such a propagation path can be considered as short-distance propagation. The minima in the diurnal phase and amplitude patterns generally occur when the solar terminator moves along the VLF propagation path (the day–night boundary is nearly perpendicular to the transmitter–receiver direction). It is a well-known fact (Galejs, 1971). One minimum takes place around sunrise, and can be named morning "terminator time" (TT); another takes place around sunset, and can be named as evening TT. Their difference value must be changed from day to day as the day length at the given geographic latitude, if the propagation path is latitudinal. In the case of earthquake influence, there occurred the abnormal behaviour of this morning and evening TT difference, which began a few days before the earthquake such that it had lengthening of daytime conditions (Hayakawa et al., 1996a,b; Molchanov and Hayakawa, 1998; Molchanov et al., 1998; Hayakawa, 2001). We assume that this abnormal behaviour of morning and evening TT difference is bound up with emergence of a local ionosphere inhomogeneity just above the earthquake epicentre, and we are going to confirm this assumption by mathematical modelling results.

The attempts of theoretical explanation of observed result on the deformation of amplitude and phase diurnal curves made to date are based on the two-dimensional solutions of the propagation problem in an irregular Earth–ionosphere waveguide. In this paper just as Soloviev et al. (2004) we present a solution of the three-dimensional subionospheric radio wave propagation problem. As in the experiment described in Hayakawa et al. (1996a,b) we will have an interest in short enough paths (≈1000 km). The scales of three-dimensional local lower ionosphere inhomogeneity (longitudinal, transverse and vertical) are chosen to be less than the terminator transition length.

2. Formulation of the propagation problem

Modelling the effects of the solar terminator is a special problem in the theory of subionospheric VLF propagation that has been often discussed in the literature. The problem of subionospheric radio wave propagation in the presence of a localized irregularity has also been discussed for a long time. In Soloviev et al. (2004) we have given a detailed list of publications devoted to modelling the effect of the solar terminator transition and separately the effect of three-dimensional ionospheric irregularities on the near-Earth propagation of radio waves.

This paper puts forward a three-dimensional modelling of radio wave propagation in an irregular waveguide with localized inhomogeneity on the terminator background. The first step of radio wave propagation problem statement is the construction of effective terrestrial waveguide model. We consider the propagation problem in some model space, which is vacuum cavity with impedance waveguide boundaries with following parameters: $\delta_g, \hat{\delta}_{it}, z_{it}, \hat{\delta}_p, z_p$. These parameters mean: δ_g – is the ground surface impedance that is determined by Earth surface reflection properties, $\hat{\delta}_{it}$ and $z_{it} = z_{it}(r, \varphi)$ are tensor impedance and function of waveguide height for the ionosphere without any local perturbation (only solar terminator transition is taken into account), $\hat{\delta}_p$ and $z_p = z_p(r, \varphi)$ are tensor impedance and surface equation of the ionospheric waveguide wall with a local perturbation on the terminator background. Suppose we have a cylindrical reference coordinate system (r, φ, z). The geometry of the effective propagation medium is presented in Fig. 1. Such an impedance waveguide model has the right to exist in very low frequency (VLF) range. The Earth's surface we will consider as uniform all through the propagation path and characterized by homogeneous surface impedance $\delta_g = \text{const}$. The tensor ionospheric surface impedance $\hat{\delta}_{it}$ and waveguide height z_{it} for the terminator transition model are obtained from the given electron

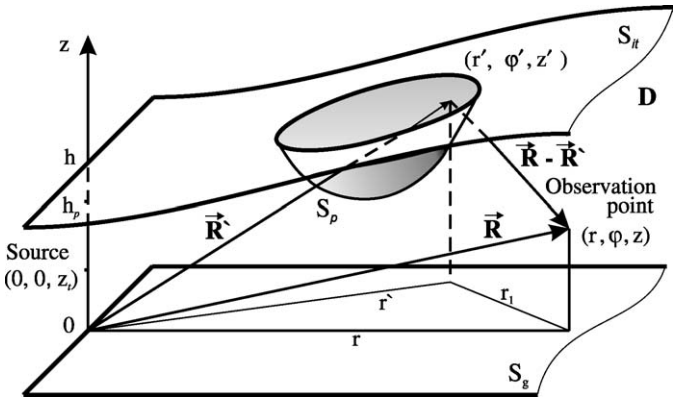

Fig. 1. Geometry of the effective propagation medium.

density $N_e(z, \Psi)$ and effective collision frequency $\nu_e(z, \Psi)$ altitude profiles (Orlov et al., 2000; Earth's Lower Ionosphere, 1995), which depend on the solar zenith angle Ψ that varies from 80° to 100° with step equal to 2°. It means that we explore the terminator transition with about 2500 km. The examples of such altitude profiles predicted for January 1995 and for central point of Tsushima–Inubo propagation path are presented in Fig. 2, the electron density altitude profiles in the upper panel, and the effective electron collision frequency in the lower panel. The two curves in the upper panel correspond to different solar zenith angle, one is for $\Psi = 80°$ (Day electron density) and the other for $\Psi = 100°$ (Night electron density). Only one effective collision frequency altitude profile is used for all $80° \leqslant \Psi \leqslant 100°$ (Fig. 2, lower panel). The impedance $\hat{\delta}_p$ and effective height z_p in a case when a locally perturbed domain is considered could be obtained from given $N_{ep}(z; r, \varphi)$ and $\nu_{ep}(z; r, \varphi)$ – altitude profiles of electron density and collision frequency for earthquake precursor disturbed ionosphere, but they are unknown to us. We require that the functions $z_{it} = z_{it}(r, \varphi)$ and $\hat{\delta}_{it} = \hat{\delta}_{it}(r, \varphi, z_{it})$ do not change in the direction perpendicular to the terminator movement direction. These functions z_{it} and $\hat{\delta}_{it}$ defining ionosphere terminator transition model are computed allowing for the geomagnetic field influence. Upon a ground of the solar terminator a three-dimensional local ionosphere inhomogeneity S_p is set above the propagation line. This last one we present as a bell-shaped perturbation of the ionospheric waveguide wall, whose centre is situated above the given point of the Earth's surface and whose lateral dimensions are less than the solar terminator transition length. The local ionosphere inhomogeneity S_p deforms the surface $S_{it}(z_{it} = z_{it}(r, \varphi))$ into the surface S_i, described by the function $z_p = z_p(r, \varphi)$ and with tensor impedance $\hat{\delta}_p = \hat{\delta}_p(r, \varphi, z_p)$. Thus, the surfaces S_{it} and S_i coincide everywhere with the exception of the area $S_p \in S_i$, which defines the surface of the local inhomogeneity.

We study a harmonic $\exp(-i\omega t)$ point source field in the three-dimensional domain D bounded by two surfaces S_g

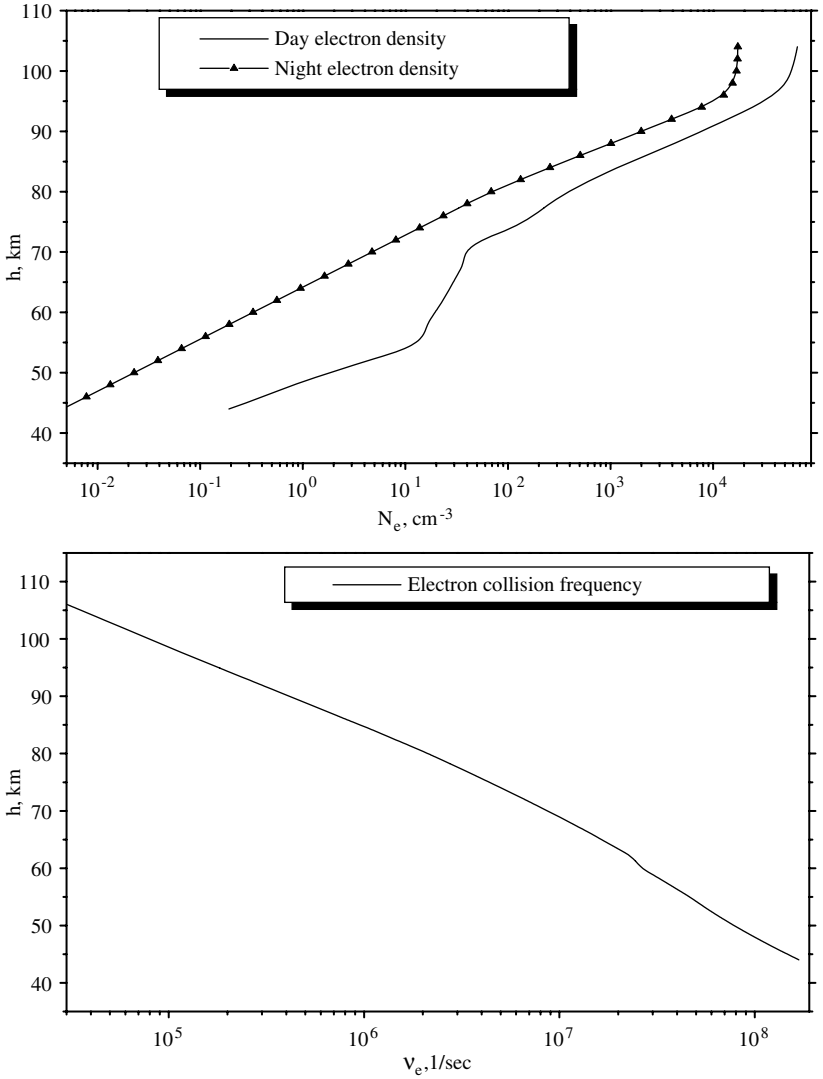

Fig. 2. The examples of electron density (upper panel) and effective collision frequency (lower panel) altitude profiles that are used to calculate the effective terrestrial waveguide model parameters.

and S_i. The source is assumed to be an electric dipole with moment P_0 located at the point described as $(x=0, y=0, z=z_t)$ in the Cartesian reference coordinate system and as $(r=0, \varphi=0, z=z_t)$ in the already-introduced cylindrical coordinate system. The dipole is chosen to be directed along the axis OZ. The surface S_g is specified as $z=0$. In the model we neglect the Earth's curvature (because our propagation path is not too long).

In vacuum the arbitrary electromagnetic field may be represented as a sum of transverse magnetic (TM) and transverse electric (TE) fields. The first may be described by the single component electrical Hertz's vector $\vec{\Pi}^{(e)} = \Pi^{(e)} e_z$, the second by the magnetic Hertz's vector $\vec{\Pi}^{(m)} = \Pi^{(m)} e_z$. The electromagnetic field components may be expressed by the following well-known formulas (e.g., Makarov et al., 1994):

$$\vec{E} = \mathrm{rotrot}\,\vec{\Pi}^{(e)} + \mathrm{i}\omega\mu_0\,\mathrm{rot}\,\vec{\Pi}^{(m)},$$

$$\vec{H} = -\mathrm{i}\omega\varepsilon_0\,\mathrm{rot}\,\vec{\Pi}^{(e)} + \mathrm{rotrot}\,\vec{\Pi}^{(m)}.$$

If we define the boundary conditions on the surfaces S_g and S_i as

$$\vec{E}_{\tan} = Z_0\hat{\delta}[\vec{H}_{\tan}\times\vec{n}],$$

where $Z_0 = \sqrt{\mu_0/\varepsilon_0}$, $\vec{n}$ is the outside normal to the waveguide volume D; $\vec{E}_{\tan}, \vec{H}_{\tan}$ are the components tangential to waveguide bound surface of the electromagnetic fields $\vec{E}$ and $\vec{H}$; $\hat{\delta} = \delta_g \cdot \hat{I}$ on the surface S_g, $\hat{I}$ is identity matrix, and $\hat{\delta} = \hat{\delta}_p = \begin{pmatrix} \delta^{(e)} & \delta_{12} \\ \delta_{21} & \delta^{(m)} \end{pmatrix}$ on the surface S_i, then for homogeneous condition it helds:

$$\frac{\partial}{\partial n}\begin{pmatrix} \Pi^{(e)} \\ Z_0\Pi^{(m)} \end{pmatrix} = \mathrm{i}k\begin{pmatrix} \delta^{(TM)}, & \frac{-\delta_{12}}{\delta^{(m)}} \\ \frac{\delta_{21}}{\delta^{(m)}}, & \frac{1}{\delta^{(m)}} \end{pmatrix} \times \begin{pmatrix} \Pi^{(e)} \\ Z_0\Pi^{(m)} \end{pmatrix}, \tag{1}$$

where $k = \omega\sqrt{\varepsilon_0\mu_0}$ is the free-space wave number, $\delta^{(TM)} = \delta^{(e)} - \delta_{12}\delta_{21}/\delta^{(m)}$. The boundary condition (1) we apply in our problem, is based on considering that components of tensor $\hat{\delta}_p$ are coordinate-dependent functions. Additionally, $\Pi^{(e)}(r,\varphi,z)$ and $\Pi^{(m)}(r,\varphi,z)$ must comply with Helmholtz equations with the point source on the right side of the equation for $\Pi^{(e)}$, and without the source on the right side of the equation for $\Pi^{(m)}$. The infinity condition requires $\Pi^{(e)}$ and $\Pi^{(m)}$ to vanish as $r\to\infty$.

3. Construction of the problem solution

Using the second Green's formula, the problem for two differential equations may be reduced to a set of coupled integral equations over the surface S_i:

$$\Pi^{(e)}(\vec{R}) = \Pi_0^{(e)}(\vec{R}) + \frac{\mathrm{i}k}{2\pi}\int\int_{S_i} W^{(e)}(\vec{R},\vec{R}')\left\{\Pi^{(e)}(\vec{R}')\left(\delta^{(TM)} + \mathrm{i}\frac{\partial W^{(e)}(\vec{R},\vec{R}')}{kW^{(e)}(\vec{R},\vec{R}')\partial n'}\right) - \frac{\delta_{12}}{\delta^{(m)}}Z_0\Pi^{(m)}(\vec{R}')\right\}\mathrm{d}S', \tag{2}$$

$$\Pi^{(m)}(\vec{R}) = \frac{\mathrm{i}k}{2\pi}\int\int_{S_i} W^{(m)}(\vec{R},\vec{R}') \times\left\{\Pi^{(m)}(\vec{R}')\left(\frac{1}{\delta^{(m)}} + \mathrm{i}\frac{\partial W^{(m)}(\vec{R},\vec{R}')}{kW^{(m)}(\vec{R},\vec{R}')\partial n'}\right) + \frac{\delta_{21}}{\delta^{(m)}}\frac{\Pi^{(e)}(\vec{R}')}{Z_0}\right\}\mathrm{d}S', \tag{3}$$

where $\vec{R}(r,\varphi,z)\notin S_i$ is the observation point, $\vec{R}'(r',\varphi',z')\in S_i$ is an integration point, $\Pi_0^{(e)}(\vec{R})$ is the vertical electric dipole field in the regular plane waveguide with height h ($h \geqslant z_p$, that means h should be more than the altitude of S_i above earth-level) and homogeneous boundary surfaces with impedances $\delta_g = \mathrm{const}$ on the ground and some $\delta^{(TM)} = \delta_0^{(TM)} = \mathrm{const}$ on the upper waveguide wall. The vector problem requires the use of a two-component Green's function, whose two components $W^{(e)}(\vec{R},\vec{R}')$ and $W^{(m)}(\vec{R},\vec{R}')$ are the solutions of the following problems:

$$\Delta W^{(e)}(\vec{R},\vec{R}') + k^2W^{(e)}(\vec{R},\vec{R}') = -2\pi\delta(x-x',y-y',z-z'),$$

$$\frac{\partial W^{(e)}}{\partial z} = -\mathrm{i}k\delta_g W^{(e)} \text{ for } z=0, \quad \frac{\partial W^{(e)}}{\partial z} = \mathrm{i}k\delta_0^{(TM)}W^{(e)} \text{ for } z=h;$$

$$\Delta W^{(m)}(\vec{R},\vec{R}') + k^2W^{(m)}(\vec{R},\vec{R}') = -2\pi\delta(x-x',y-y',z-z'),$$

$$\frac{\partial W^{(m)}}{\partial z} = -\frac{\mathrm{i}k}{\delta_g}W^{(m)} \text{ for } z=0, \quad \frac{\partial W^{(m)}}{\partial z} = \frac{\mathrm{i}k}{\delta_0^{(m)}}W^{(m)} \text{ for } z=h,$$

$W^{(e)}(\vec{R},\vec{R}') = W^{(e)}(\vec{R}_1)$ and $W^{(m)}(\vec{R},\vec{R}') = W^{(m)}(\vec{R}_1)$ where $\vec{R}_1 = \vec{R} - \vec{R}'$ and $r_1 = \sqrt{r^2 + r'^2 - 2rr'\cos(\varphi-\varphi')}$ (see Fig. 1); $\delta_0^{(m)}$ is some constant impedance.

The algorithm to solve the set of Eqs. (2) and (3) may be the following. First of all we transform the surface integrals from right-hand side of Eqs. (2) and (3), which are surface integrals of the first type (Fihtenholtz, 1969), into ordinary two-dimensional integrals over $z=\mathrm{const}$ plane:

$$\int\int_{S_i} f(x',y',z')\,\mathrm{d}S' = \int\int_{\Omega_i} f(x',y',z_p'(x',y'))\sqrt{1+p^2+q^2}\,\mathrm{d}x'\,\mathrm{d}y'.$$

Here, Ω_i is the (x,y) plane projection of the surface S_i; $p = \frac{\partial z_p'(x',y')}{\partial x'}$, $q = \frac{\partial z_p'(x',y')}{\partial y'}$. We separate the plane Ω_i into two parts: Ω_p and Ω_∞ ($\Omega_i = \Omega_p \cup \Omega_\infty$), where the first Ω_p is the (x,y) plane projection of the local perturbation surface S_p while for the second, which is the all-remaining part of the plane Ω_i, we have the coincidence of the functions z_p and z_{it} and $\hat{\delta}_p$ and $\hat{\delta}_{it}$, i.e. for $x,y\in\Omega_\infty$ we have $z_p(x,y) = z_{it}(x,y)$, and $\hat{\delta}_p(x,y,z) = \hat{\delta}_{it}(x,y,z)$ (see Fig. 3).

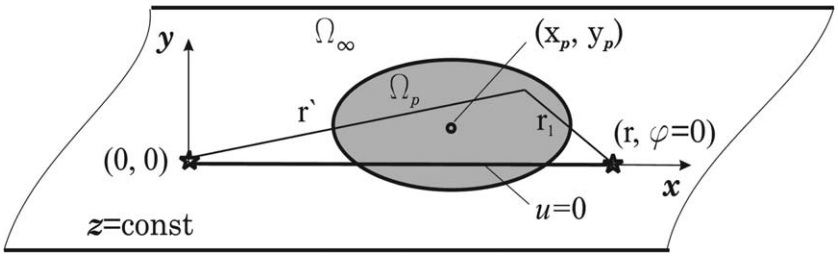

Fig. 3. Geometry of the problem, top view.

We can rewrite Eq. (2) in an equivalent form:

$$\begin{aligned}\Pi^{(e)}(\vec{R}) &= \Pi_0^{(e)}(\vec{R}) \\ &+ \frac{ik}{2\pi}\int\int_{\Omega_p+\Omega_\infty} W^{(e)}\left\{\Pi^{(e)}(\vec{R}')\left(\delta_t^{(TM)} + i\frac{\partial \ln W^{(e)}}{k\partial n'}\right)\right. \\ &\left. - \frac{\delta_{12}^t}{\delta_t^{(m)}} Z_0 \Pi^{(m)}(\vec{R}')\right\}\sqrt{1+p_t^2+q_t^2}\,dx'\,dy' \\ &+ \frac{ik}{2\pi}\int\int_{\Omega_p} W^{(e)}\left\{\left(\Pi^{(e)}(\vec{R}')\left(\delta^{(TM)} + i\frac{\partial \ln W^{(e)}}{k\partial n'}\right)\right.\right. \\ &\left. - \frac{\delta_{12}}{\delta^{(m)}} Z_0 \Pi^{(m)}(\vec{R}')\right)\sqrt{1+p^2+q^2} \\ &- \left(\Pi^{(e)}(\vec{R}')\left(\delta_t^{(TM)} + i\frac{\partial \ln W^{(e)}}{k\partial n'}\right)\right. \\ &\left.\left. - \frac{\delta_{12}^t}{\delta_t^{(m)}} Z_0 \Pi^{(m)}(\vec{R}')\right)\sqrt{1+p_t^2+q_t^2}\right\} dx'\,dy', \end{aligned} \quad (4)$$

where $\delta_t^{(TM)}, \delta_{12}^t, \delta_t^{(m)}$ are the components of tensor $\hat{\delta}_{it}$; $p_t = \frac{\partial z'_{it}(x',y')}{\partial x'}$, $q_t = \frac{\partial z'_{it}(x',y')}{\partial y'}$, $\vec{R} \notin S_i$.

This allows us to distinguish the integral over the surface of local inhomogeneity Ω_p in separate term. In a limiting case $\vec{R} \to S_i$ additional terms arise such as $\Pi^{(e)}(\vec{R})/2$ on the right-hand side of Eq. (4) and $\Pi^{(m)}(\vec{R})/2$ on the right-hand side of Eq. (3) due to the jump of the normal derivatives of the Green's function components $\partial W^{(e)}(\vec{R}', \vec{R})/\partial n'$ and $\partial W^{(m)}(\vec{R}', \vec{R})/\partial n'$.

To solve the set of Eqs. (3) and (4), we apply the asymptotic method (Soloviev, 1998). We begin with introducing the slowly varying attenuation functions $V^{(e)}$(electric), $V^{(m)}$(magnetic) and $V_0^{(e)}$:

$$\Pi^{(e)}(\vec{R}) = \frac{P_0}{2\pi\varepsilon_0}\frac{e^{ikr}}{r}V^{(e)}(\vec{R}), \quad \Pi^{(m)}(\vec{R}) = \frac{-P_0}{2\pi\sqrt{\mu_0\varepsilon_0}}\frac{e^{ikr}}{r}V^{(m)}(\vec{R}),$$

$$W^{(e)}(\vec{R},\vec{R}') = \frac{e^{ikr_1}}{r_1}V_0^{(e)}(\vec{R},\vec{R}'). \quad (5)$$

Then we introduce on the surface (x,y) an elliptic coordinate system (u,v) with focuses at the points: the origin $(0,0)$ and observation point plane projection $(r,0)$:

$$x' - \frac{r}{2} = \frac{r}{2}\operatorname{ch}u\cos v, \quad y' = \frac{r}{2}\operatorname{sh}u\sin v,$$
$$dx'\,dy' = r'r_1\,du\,dv, \quad -\infty < u < +\infty, \ 0 \leqslant v \leqslant \pi.$$

After substitution of the variables of integration we arrive at a set of Eqs. (6) and (7) for the slowly varying attenuation functions $V^{(e)}$ and $V^{(m)}$:

$$\begin{aligned}V^{(e)}(\vec{R}) &= V_0^{(e)}(\vec{R}) + \frac{ikr}{2\pi}\int\int_{\Omega_i} f_t^{(em)}(\vec{R},u,v)e^{ikr(\operatorname{ch}u-1)}\,du\,dv \\ &+ \frac{ikr}{2\pi}\int\int_{\Omega_p} f^{(em)}(\vec{R},u,v)e^{ikr(\operatorname{ch}u-1)}\,du\,dv, \end{aligned} \quad (6)$$

$$V^{(m)}(\vec{R}) = \frac{ikr}{2\pi}\int\int_{\Omega_i} f^{(me)}(\vec{R},u,v)e^{ikr(\operatorname{ch}u-1)}\,du\,dv. \quad (7)$$

If we suppose $kr \gg 1$, the exponential factor $e^{ikr(\operatorname{ch}u-1)}$ may be assumed as being rapidly oscillating with respect to u (across the wave propagation path) as compared with the remaining cofactors $f_t^{(em)}(\vec{R},u,v)$, $f^{(em)}(\vec{R},u,v)$ and $f^{(me)}(\vec{R},u,v)$. This allows us to use the method of stationary phase for calculating the integrals over u. Before we apply the method of stationary phase, we need to transform the integrals from Eqs. (6) and (7). Eqs. (8)–(10) present the sequential steps of this operation:

$$\int\int_{\Omega_i} \ldots du\,dv = \int_0^\pi \left(\int_{-\infty}^{+\infty} \ldots du\right) dv, \quad (8)$$

$$\int\int_{\Omega_p} \ldots du\,dv = \int_{v_<}^{v_>} \left(\int_{u_<(v)}^{u_>(v)} \ldots du\right) dv, \quad (9)$$

$$\int_{u_<(v)}^{u_>(v)} \ldots du = \int_{u_<(v)}^{\infty} \ldots du - \int_{u_>(v)}^{\infty} \ldots du. \quad (10)$$

The line $u = 0$ which connects the plane projections of the source and the observation points, is a stationary phase point for infinite and semi-infinite integrals. To avoid losing the information on the transverse structure of the inhomogeneity, we must perform the stationary phase calculations with accuracy up to the terms of order $O((kr)^{-1})$, neglecting only higher-order terms $O((kr)^{-3/2})$. Thus, we have

$$\int_{-\infty}^{+\infty} f_t^{(em)}(\vec{R},u,v)e^{ikr(\operatorname{ch}u-1)}\,du \approx f_t^{(em)}(\vec{R},0,v)i\pi H_0^{(1)}(kr), \quad (11)$$

$$\begin{aligned}\int_{u(v)}^{\infty} f^{(em)}(\vec{R},u,v)e^{ikr(\operatorname{ch}u-1)}\,du &\approx \frac{\exp[ikr(\operatorname{ch}u(v)-1)]}{i\sqrt{2kr}} \\ &\times G(\vec{R},u(v),v) + O[(kr)^{-3/2}], \end{aligned} \quad (12)$$

where $H_0^{(1)}(kr)$ is Hankel's function,

$$G[\vec{R},u(v),v] = \sqrt{\pi}\mathrm{e}^{\mathrm{i}3\pi/4} f^{(\mathrm{em})}(\vec{R},0,v) w(\mathrm{e}^{\mathrm{i}\pi/4} g) + \frac{1}{g}\left[f(\vec{R},0,v) - \frac{f(\vec{R},u(v),v)}{\mathrm{ch}(u(v)/2)}\right],$$

$$g = \sqrt{2kr}\,\mathrm{sh}\left(\frac{u(v)}{2}\right),$$

$w(x) = \mathrm{e}^{x^2}\left[1 + (2\mathrm{i}/\sqrt{\pi})\int_0^x \mathrm{e}^{t^2}\,\mathrm{d}t\right]$ is the conventional probability integral of a complex variable (Abramowitz and Stegun, 1964). As a result of stationary phase calculations we arrive at the set of two coupled one-dimensional equations (instead of one in Soloviev et al. (2004)) with contour integrals along two lines: the (x,y) plane projection of the propagation line ($u = 0, 0 < v < \pi$) and the linear boundary $\partial\Omega_p$ ($u = u(v)$) of the local inhomogeneity area. In an operator form this is the following set of equations for electric $V^{(\mathrm{e})}$ and magnetic $V^{(\mathrm{m})}$ attenuation functions:

$$V^{(\mathrm{e})} = V_0^{(\mathrm{e})} + A_\mathrm{e} \times V^{(\mathrm{e})} + B_\mathrm{e} \times V^{(\mathrm{e})} + C_\mathrm{e} \times V^{(\mathrm{m})}, \quad (13)$$

$$V^{(\mathrm{m})} = A_\mathrm{m} \times V^{(\mathrm{m})} + B_\mathrm{m} \times V^{(\mathrm{m})} + C_\mathrm{m} \times V^{(\mathrm{e})}, \quad (14)$$

where $A_{\mathrm{e,m}}$ are Volterra operators, $B_{\mathrm{e,m}}$ and $C_{\mathrm{e,m}}$ are Fredholm operators. To solve the set of integral equations (13) and (14), we use the numerical–analytical method of semi-inversion (Soloviev and Agapov, 1997). The algorithm of solution is the formulas (15) and (16):

$$V_j^{(\mathrm{e})} = (I - A_\mathrm{e})^{-1} \times \left(V_0^{(\mathrm{e})} + B_\mathrm{e} \times V_{j-1}^{(\mathrm{e})} + C_\mathrm{e} \times V_{j-1}^{(\mathrm{m})}\right), \quad (15)$$

$$V_j^{(\mathrm{m})} = (I - A_\mathrm{m})^{-1} \times \left(B_\mathrm{m} \times V_{j-1}^{(\mathrm{m})} + C_\mathrm{m} \times V_j^{(\mathrm{e})}\right), \quad (16)$$

where $j = 1,2,3,\ldots$ is iteration number, $V_0^{(\mathrm{m})} = 0$. Then, for example, $V_1^{(\mathrm{e})} = (I - A_\mathrm{e})^{-1} \times (V_0^{(\mathrm{e})} + B_\mathrm{e} \times V_0^{(\mathrm{e})})$ and $V_1^{(\mathrm{m})} = (I - A_\mathrm{m})^{-1} \times C_\mathrm{m} \times V_1^{(\mathrm{e})}$. We point out that converted operators $(I - A_{\mathrm{e,m}})^{-1}$ can be found by the conventional stepwise procedure (e.g., Wagner, 1954). Moreover, any one of them contains the first dominant term of the asymptotic expansion. In comparison with $B_{\mathrm{e,m}}$, and $C_{\mathrm{e,m}}$ their contributions to the solution are expected to be more significant for a larger value of the parameter kr.

For calculating the field in a uniform waveguide ($\Pi_0^{(\mathrm{e})}(\vec{R})$, $W^{(\mathrm{e})}(\vec{R},\vec{R}')$ and $W^{(\mathrm{m})}(\vec{R},\vec{R}')$) a computer program was created, which computes the absolute value and argument of attenuation function of the vertical component of Hertz's vectors for any $0 \leqslant z_t, z \leqslant h$ and $r \geqslant 0$ with a preassigned precision. It is full-wave presentation that combines both the ray-expansion method and the normal mode series.

4. Numerical results and discussion

For the numerical simulation of radio wave propagation process on the Tsushima–Inubo path (Hayakawa et al., 1996a,b) we choose the following values of Earth–ionosphere waveguide model: Earth's surface properties are defined by $\sigma = 4.0 S/m$, $\varepsilon_r = 81$ and the path length is about $R \sim 1000$ km. We have calculated tensor impedance $\hat{\delta}_{it}$ and z_{it} from the given electron density $N_\mathrm{e}(z)$ and effective collision frequency $\nu_\mathrm{e}(z)$ altitude profiles, following the technique explicitly described for isotropic case by Soloviev and Hayakawa (2002). The components of tensor $\hat{\delta}_{it}$ and z_{it} are the solutions to the problem of a plane wave obliquely incident to the vertically inhomogeneous half-space with anisotropic ionospheric plasma, with allowing for the geomagnetic field. The components of tensor $\hat{\delta}_{it}$ satisfy the matrix Riccati equation. The effective altitude in each cross-section of inhomogeneous guide z_{it} is obtained from the condition that the calculated impedance value $\delta_{it}^{(\mathrm{TM})}$ most weakly depends upon the angle of incidence of the plane wave that is appropriate to the main eigenvalue of regular impedance waveguide with such altitude. The validity of this inhomogeneous impedance waveguide model to a three-dimensional radio wave propagation problem was demonstrated in Soloviev (1993) by means of comparing our computational results with experimental data for VLF radio wave propagation under HF ionospheric heating (Barr et al., 1984). The components of geomagnetic field were computed in multipole approximation for central point on the path. Both the transmitter and receiver (observer location) were assumed to be on the Earth's surface, $z_t = z = 0$. We considered one signal frequency: $f_1 = 10.2$ kHz.

Because the perturbed ionospheric altitude profiles $N_\mathrm{ep}(z)$ and $\nu_\mathrm{ep}(z)$ are unknown to us, we simulate the local ionospheric disturbance as a bell-shaped perturbation of the waveguide ionospheric bound:

$$\Delta h = A_p \exp[-((x - x_p)^2 + (y - y_p)^2)/r_p^2]. \quad (17)$$

In Eq. (17) the effective radius of perturbation is chosen equal to $r_p = 200$ km; the position of the disturbance centre with respect to the propagation path corresponds to the great Hyogo-ken Nambu (Kobe) earthquake (January 17, 1995) epicentre and is determined by the following values of the horizontal coordinates $x_p = 464$ km and $y_p = -70$ km (see Fig. 3). On the basis of our previous paper (Soloviev et al., 2004) we have considered the model disturbances as some depression of upper waveguide bound without any impedance variation, when $A_p = -3$ km, $\delta_p(r,\varphi, z_{it} + \Delta h) = \delta_i(r,\varphi,z_{it})$. The concrete value of A_p was chosen from the interval $0 \leqslant |A_p| < (z_{\mathrm{it\,night}} - z_{\mathrm{it\,day}})$.

Results of numerical simulation are presented only for electric attenuation function $V^{(\mathrm{e})}$, excited by initial source – vertical electric dipole. Magnetic attenuation function $V^{(\mathrm{m})}$ describing the secondary component of electromagnetic field, whose occurrence is obliged to the scattering by an anisotropic upper waveguide bound, has not been analysed. It means that the results of the present paper should be considered as preliminary.

Besides the basic propagation path Tsushima–Inubo, whose direction over the geomagnetic field direction is defined by an azimuth $A = 82°$, we have considered other propagation paths with azimuth values equal to $A = 45°$ and $A = 135°$. All figures present the sunrise situation.

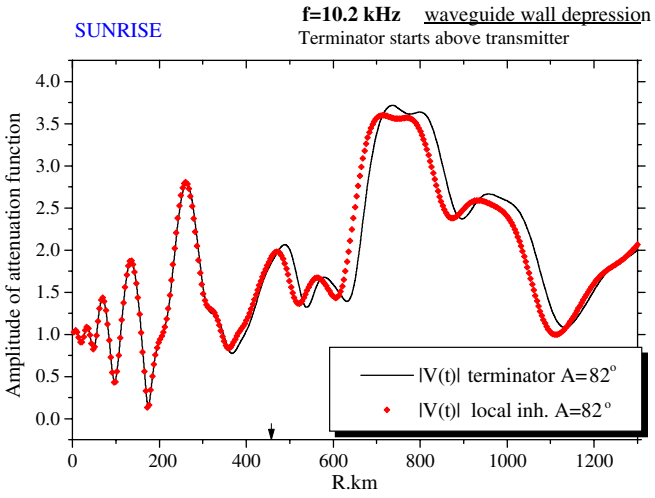

Fig. 4. Amplitude of attenuation function as a function of distance from the transmitter. The propagation path direction corresponds to azimuth $A = 82°$.

Fig. 4 illustrates the behaviour of amplitude of attenuation function $V^{(e)}$ as a function of distance from the transmitter. The perturbation of the ionospheric waveguide bound is waveguide wall depression. Solar terminator starts above the transmitter location. Hereafter, and in the all-succeeding figures, there are one or more couples of curves in each panel; in each couple the solid line corresponds to the situations without any local inhomogeneity above the propagation path (only taking into account the terminator transition), and the dotted line corresponds to the problem with local inhomogeneity (local inhomogeneity against the background of terminator transition). In the pattern an arrow indicates the longitudinal coordinate value that corresponds to local ionosphere disturbance centre location. As we can see, the emergence of such a perturbation on the propagation path disturbs the amplitude of attenuation function. This disturbance is noticeable both at the points $x < x_p$, and at $x > x_p$, anyway, up to $x \approx$ 1150 km.

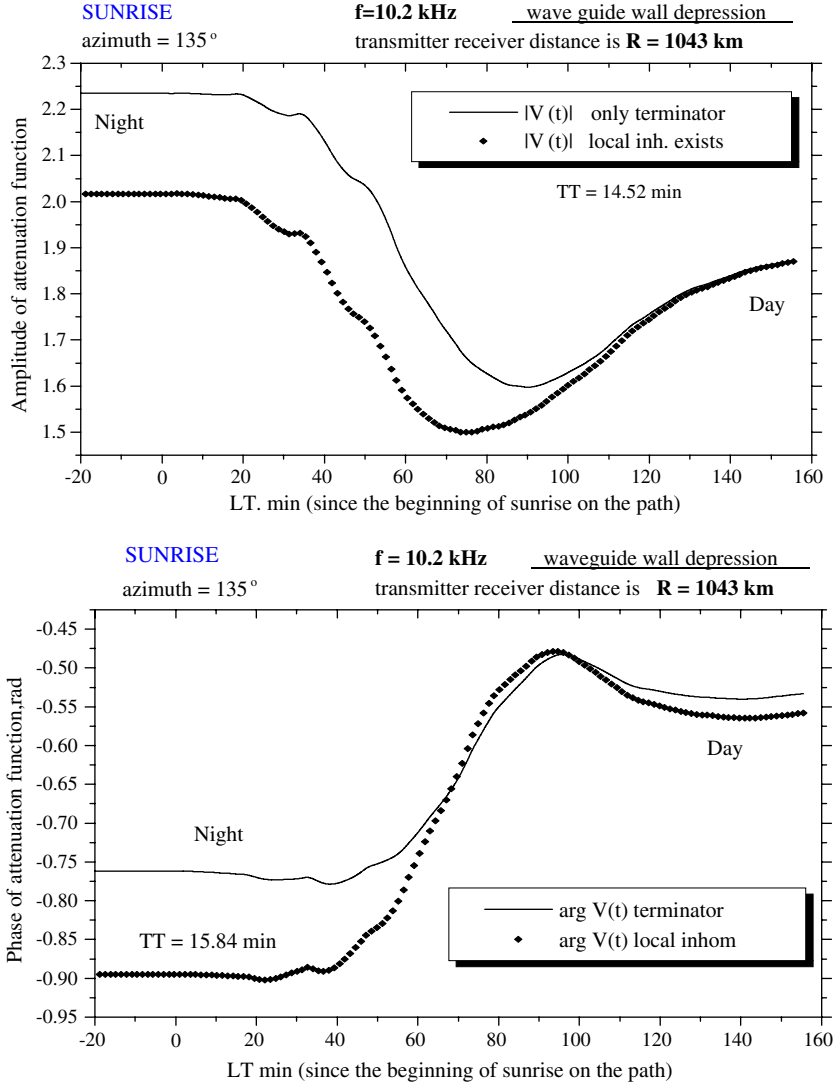

Fig. 5. Amplitude (upper panel) and phase (lower panel) of attenuation function as a functions of local time (LT) since the beginning of sunrise on the path. The propagation path direction corresponds to azimuth $A = 135°$.

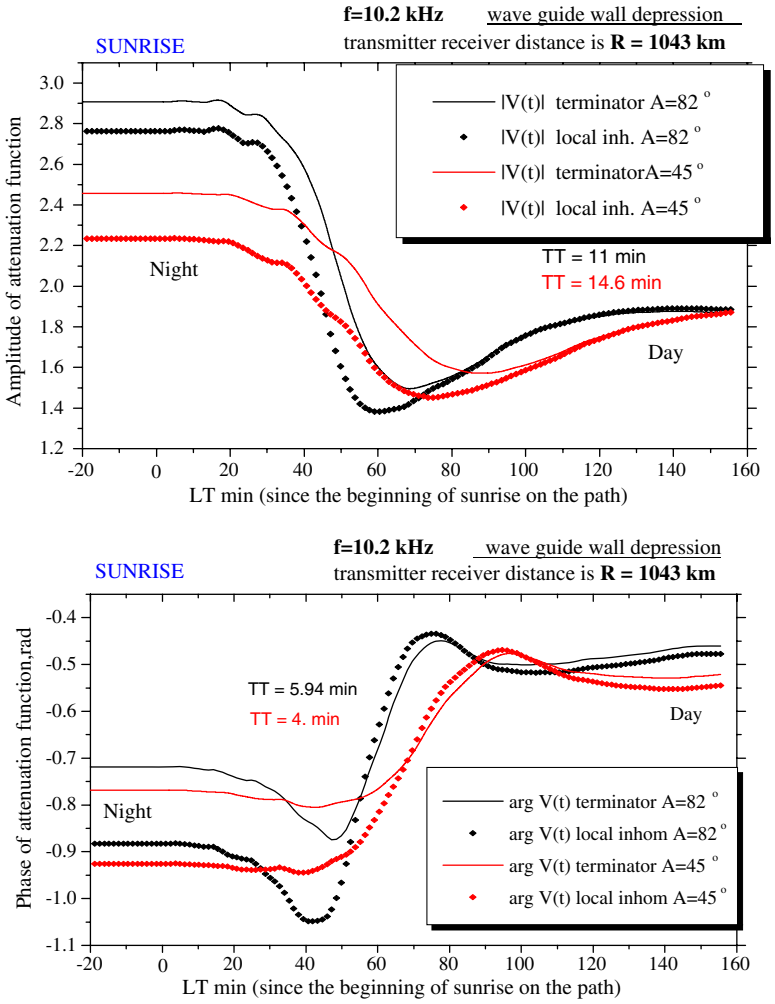

Fig. 6. Amplitudes (upper panel) and phases (lower panel) of attenuation function as functions of local time (LT) since the beginning of sunrise on the path. Two different propagation paths corresponding to different azimuths $A = 82°$ and $A = 45°$.

Fig. 5 shows the behaviour of amplitudes (in the upper panel) and phases (in the lower panel) of attenuation function as functions of local time (LT) since the beginning of sunrise on the path. The transmitter–receiver distance is 1043 km. The azimuth of propagation is $A = 135°$. The shift in the amplitude as well as in the phase minimum on the side of lengthening of the day conditions may be seen in both the patterns. These shifts are found to be around and more than 15 min (TT).

Fig. 6 contains two couples of curves. One of them corresponds to the propagation path with azimuth $A = 82°$, another to the path with azimuth $A = 45°$. The upper panel illustrates the behaviour of amplitudes of attenuation function as functions of local time (LT) since the beginning of sunrise on the path. The lower panel shows the behaviour of phases of attenuation function as functions of local time (LT) since the beginning of sunrise on the path. The deviation in amplitude (upper panel) and phase (lower panel) minima may be evidently defined in each panel and for different propagation path directions. The deviations for amplitude (TT > 10 min) is more than for phase (TT ≈ 5 min), but always in the same tendency of lengthening of the day conditions.

5. Conclusions

The investigation of various propagation paths, which cut across the terminator line at different angle (different azimuths A), has shown that the emergence of a local ionosphere inhomogeneity on the radio wave propagation across the Solar terminator path deforms the diurnal curves of VLF field amplitude and phase in accordance with the above-mentioned observational data (Hayakawa et al., 1996a,b). This local inhomogeneity must be equivalent to the local waveguide wall depression and not the local waveguide wall elevation (Soloviev et al., 2004). In this case only the shift in the amplitude or phase minima is on the side of lengthening of the day conditions (as in the experiment). It is possible to ascertain that the specified property is kept for propagation paths having different orientations with respect to a direction of geomagnetic field vector, anyway for azimuth interval $45° \leqslant A \leqslant 135°$. This

effect is a result of interaction of multimode field with the complicated waveguide boundary.

Acknowledgements

We are grateful to V.I. Ivanov for help in numerical codes debugging. The first author (O.V.S) is thankful to the University of Electro-Communications for having given him an opportunity to visit Japan for the joint research with Japanese colleagues. One of authors (M. H.) is grateful to The Mitsubishi Foundation, JSPS (#15403012) and NiCT (R&D promotion scheme funding international joint research) for their support.

References

Abramowitz, M., Stegun, I., 1964. Handbook of Mathematical Functions. U.S. Gov. Print. Off., Washington, DC.

Barr, R., Rietveld, M.T., Kopka, H., Stubbe, P., 1984. Effect of a heated patch of auroral ionosphere on VLF-radio wave propagation. Nature 309 (5968), 534–536.

Earth's Lower Ionosphere, 1995. The model of the global distribution of electron density and effective collision frequency for low-frequency radio wave propagation (electromagnetic field) prediction. GOST R 25645.157-94. Standards Press, Moscow, 380 pp.

Fihtenholtz, G.M., 1969. Course in the Differential and Integral Calculus, vol. III. Nauka, Moscow.

Galejs, J., 1971. VLF propagation across discontinuous day-time to night-time transitions in anisotropic terrestrial waveguide. IEEE Trans. Ant. Prop. 19, 756–762.

Hayakawa, M., 2001. NASDA's Earthquake remote sensing frontier research; Seismo-electromagnetic phenomena in the lithosphere, atmosphere and ionosphere. Final report, p. 228.

Hayakawa, M., Molchanov, O.A. (Eds.), 2002. Seismo Electromagnetics, Lithosphere–Atmosphere–Ionosphere Coupling. TERRAPUB, Tokyo, p. 477.

Hayakawa, M., Molchanov, O.A., Ondoh, T., Kawai, E., 1996a. The precursory signature effect of the Kobe earthquake on VLF subionospheric signals. J. Comm. Res. Lab. 43, 169–180.

Hayakawa, M., Molchanov, O.A., Ondoh, T., Kawai, E., 1996b. Precursory signature of the Kobe earthquake on VLF subionospheric signal. J. Atmos. Electr. 16 (3), 247–257.

Hobara, Y., Lefeuvre, F., Parrot, M., Molchanov, O.A., 2005. Low-latitude ionospheric turbulence observed by Aureol-3 satellite. Annales Geophysicae 23 (4), 1259–1270.

Lizunov, G., Hayakawa, M., 2004. Atmospheric gravity waves and their role in the lithosphere–troposphere–ionosphere interaction. IEEJ Trans. Fund. Mater. 124 (12), 1109–1120.

Makarov, G.I., Novikov, V.V., Rybachek, S.T., 1994. Radio Wave Propagation in the Earth–Ionosphere Waveguide and in the Ionosphere. Nauka, Moskow, 152pp.

Molchanov, O.A., Hayakawa, M., 1998. Subionospheric VLF signal perturbations possibly related to earthquakes. J. Geophys. Res. 103 (A8), 17489–17504.

Molchanov, O.A., Hayakawa, M., Ondoh, T., Kawai, E., 1998. Precursory effects in the subionospheric VLF signals for the Kobe earthquake. Phys. Earth Planet. Interiors 105, 239–248.

Orlov, A.B., Pronin, A.E., Uvarov, A.N., 2000. The electron density of lower ionosphere profile modelling according to the VLF propagation data. In: Problemy Difraktsii i Rasprostraneniya, vol. 28. St. Petersburg Univ. Press, St. Petersburg, pp. 83–114.

Soloviev, O.V., 1993. Effect of a patch of ionosphere illuminated by a powerful HF transmitter on VLF radio wave propagation. Abstract, XXIV GA of URSI, Kyoto, Japan, p. 639.

Soloviev, O.V., 1998. Low frequency radio wave propagation in the Earth–ionosphere waveguide perturbed by a large-scale three-dimensional inhomogeneity. Izv. Vyssh. Uchebn. Zaved. Radiofiz. 41 (5), 588–604.

Soloviev, O.V., 2005. Three-dimensional vector problem of VLF radio wave scattering by a local lower ionosphere inhomogeneity. In: Radio wave propagation: Proceedings of XXI All-Russian Scientific Conference, Yoshkar-Ola, vol. 1, pp. 447–451.

Soloviev, O.V., Agapov, V.V., 1997. An asymptotic three-dimensional technique to study radio wave propagation in the presence of a localized perturbation of environment. Radio Sci. 32 (2), 515–524.

Soloviev, O.V., Hayakawa, M., 2002. Three-dimensional subionospheric VLF field diffraction by a truncated high conducting cylinder and its application to Trimpi effect problem. Radio Sci. 37 (5). doi:10.1029/2001RS002499.

Soloviev, O.V., Hayakawa, M., Ivanov, V.I., Molchanov, O.A., 2004. Seismo-electromagnetic phenomenon in the atmosphere in terms of 3D subionospheric radio wave propagation problem. Phys. Chem. Earth 29, 639–647. doi:10.1016/j.pce.2003.10.002.

Wagner, C., 1954. On the numerical solution of Volterra integral equations. J. Math. Phys. 32 (4), 289–301.